Chemical Science

ROYAL SOCIETY OF CHEMISTRY

EDGE ARTICLE

View Article Online
View Journal | View Issue

Cite this: *Chem. Sci.*, 2020, **11**, 1636

All publication charges for this article have been paid for by the Royal Society of Chemistry

Received 25th September 2019
Accepted 23rd December 2019

DOI: 10.1039/c9sc04849a

rsc.li/chemical-science

Readily accessible sp^3-rich cyclic hydrazine frameworks exploiting nitrogen fluxionality†

Conor Dean, [a] Sundaram Rajkumar,[a] Stefan Roesner, [a] Nessa Carson, [b] Guy J. Clarkson, [a] Martin Wills, [a] Matthew Jones[c] and Michael Shipman *[a]

Increased molecular complexity correlates with improved chances of success in the drug development process. Here, a strategy for the creation of sp^3-rich, non-planar heterocyclic scaffolds suitable for drug discovery is described that obviates the need to generate multiple stereogenic centers with independent control. Asymmetric transfer hydrogenation using a tethered Ru-catalyst is used to efficiently produce a range of enantiopure cyclic hydrazine building blocks (up to 99% ee). Iterative C–N functionalization at the two nitrogen atoms of these compounds produces novel hydrazine and hydrazide based chemical libraries. Wide chemical diversification is possible through variation in the hydrazine structure, use of different functionalization chemistries and coupling partners, and controlled engagement of each nitrogen of the hydrazine in turn. Principal Moment of Inertia (PMI) analysis of this small hydrazine library reveals excellent shape diversity and three-dimensionality. NMR and crystallographic studies confirm these frameworks prefer to orient their substituents in three-dimensional space under the control of a single stereogenic center through exploitation of the fluxional behavior of the two nitrogen atoms.

1. Introduction

Libraries of small molecules capable of exploring new areas of three-dimensional chemical space are of considerable value in drug discovery. There is growing evidence that molecular complexity, as measured by parameters such as the fraction of saturated carbon atoms (Fsp^3) and number of stereogenic centers, correlates with success rates in drug development.[1,2] Despite these observations, analysis of current drug-like libraries such as the ChEMBL dataset reveals that they generally lack shape diversity and three-dimensionality.[2] Hence, there is a need to create new stereochemically-rich compound libraries for use in drug-discovery programs that overcome these shortcomings. This is a challenging problem because it necessitates moving away from well-established synthetic methods (*e.g.* sp^2–sp^2 cross-couplings) toward chemistries that efficiently create non-planar scaffolds.[3] In this Edge article, we report a way to create novel chemical libraries with considerable shape diversity without having to generate multiple stereogenic centers with independent control. The idea exploits the fluxional behavior of pyramidal nitrogen atoms within enantiopure cyclic hydrazines, to create new sp^3-rich heterocyclic frameworks that display their chirality in an orchestrated way (Scheme 1).

This approach has a number of attractive features. Cyclic hydrazines and hydrazides are well represented in medicinal chemistry.[4] They are found in many bioactive compounds including natural products (*e.g.* actinoramide A,[5] sanglifehrin A[6]), proprietary lead compounds[7] and approved drugs (*e.g.* cilazapril[8]) (Fig. 1). Chemical libraries of **1** for discovery programs should be readily available by simple, late-stage diversification of **2** by iterative functionalization at each nitrogen atom. The availability of a plethora of C–N functionalization reactions combined with the high nucleophilicity of the hydrazine

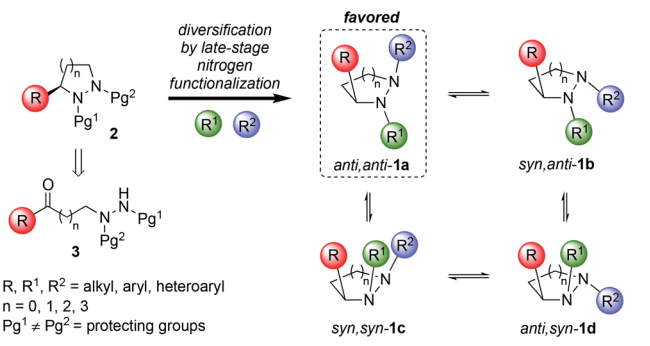

Scheme 1 New sp^3-rich cyclic hydrazine scaffolds exploiting *N*-fluxionality.

[a]*Department of Chemistry, University of Warwick, Gibbet Hill Road, Coventry, CV4 7AL, UK. E-mail: m.shipman@warwick.ac.uk*

[b]*AMRI UK, Ltd., Erl Wood Manor, Windlesham, Surrey, GU20 6PH, UK*

[c]*Eli Lilly & Company Ltd., Erl Wood Manor, Windlesham, Surrey, GU20 6PH, UK*

† Electronic supplementary information (ESI) available: Experimental procedures and characterization data for all new compounds, copies of HPLC traces, ^{1}H and ^{13}C NMR spectra, VT-NMR, PMI analysis and XRD structures. CCDC 1944266–1944273 and 1955341. For ESI and crystallographic data in CIF or other electronic format see DOI: 10.1039/c9sc04849a

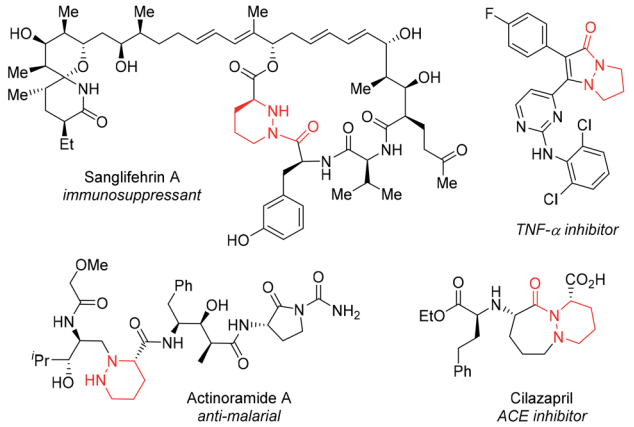

Fig. 1 Representative examples of bioactive molecules containing cyclic hydrazine and hydrazide frameworks (highlighted in red).

functional group make this disconnection highly attractive. By exploiting their dynamic behavior, it should be possible to display three substituents (R, R^1 and R^2) attached to carbon and nitrogen very precisely in three-dimensional space. Of the four conformational isomers **1a–d** that arise from pyramidal inversion, **1a** is expected to be dominant. Typically, cyclic hydrazines adopt an *anti*-configuration between the N-substituents to minimize non-bonded interactions between the lone pairs.[9] Thus, the formation of **1b** and **1c** is expected to be disfavored. Furthermore, non-bonding interactions between adjacent *syn*-substituents should disfavor **1b–d** relative to *anti*,*anti*-**1a**. Thus, control over only one stereogenic center is needed to produce predictable, non-planar frameworks. Finally, further fine-tuning of the substituent positioning should be possible by variation of the ring size.

2. Results and discussion

2.1. Asymmetric synthesis of cyclic hydrazine frameworks

The first task was to identify an efficient, enantioselective route to the hydrazine building blocks, *i.e.* **2** (Scheme 1). Key requirements for such a synthesis were that it: (i) allow the introduction of a variety of medicinally-relevant R substituents with high levels of enantiocontrol; (ii) provide access to different ring sizes; and (iii) yield differentially protected hydrazines **2** suitable for facile introduction of the R^1 and R^2 groups. While several methods for the asymmetric synthesis of cyclic hydrazines exist,[10] none met our requirements. Consequently, a new two-step approach to **2** was devised based upon enantiocontrolled reduction of ketones **3** followed by ring closure. By varying the linker length between the ketone and hydrazine functional groups, the approach offers access to a range of different ring sizes. In choosing a method for the reduction, we were drawn to Ru-catalyzed asymmetric transfer hydrogenation (ATH) which typically delivers high levels of enantioselectivity, requires low catalyst loadings, has diverse functional group compatibility and is operationally simple to perform.[11]

Initially, phenyl ketone **5a** was prepared by alkylation of readily-available, triply-protected hydrazine **4a**[12] with 2-bromoacetophenone, followed by Boc deprotection (Table 1). Where doubly-protected CbzNHNHTs is used in these alkylations, the isomeric products in which the sulfonamide and carbamate groups are transposed can also be made (for full details, see ESI†). Next, ATH reduction of **5a** was examined by screening a range of chiral diphenylethylenediamine (DPEN)/Ru(II) catalysts (**7a–g**) using formic acid and triethylamine (5 : 2 azeotrope) as hydrogen source. The majority of these reactions benefited from catalysts that were tethered between the arene and DPEN ligand.[13] Variation in the catalyst structure has a greater impact on catalytic activity than enantioselectivity (Table 1), and chlorinated solvents were found to be most effective (for details, see ESI†). Under the optimized conditions, ketone **5a** was efficiently converted into alcohol *R*-**6a** in 97% yield and 99% ee using 1 mol% of tethered ruthenium catalyst *S*,*S*-**7c** (Table 1, entry 3). The structure and absolute configuration of *R*-**6a** were confirmed by X-ray crystallography using the Flack parameter (Fig. 2, box insert).[14] The sense of asymmetric induction fits established models,[13a] indicating that the hydrazine plays no active role in catalyst binding.

Next, the ATH of a broad range of ketones was examined using the optimized conditions (Fig. 2). Full details relating to the synthesis of substrates **5a–v** are provided in the ESI.† High yields and enantioselectivities were achieved in all cases, with variations in the arene, nitrogen protecting groups and linker length well tolerated. The sense of asymmetric induction in these transformations was made by analogy to that seen for *R*-

Table 1 Optimization of Ru-catalyzed asymmetric transfer hydrogenation of ketone **5a**

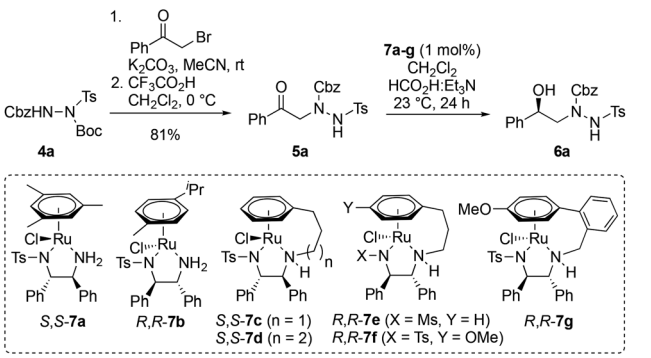

Entry	Catalyst	Yield[a] [%]	ee[b] [%]
1	*S*,*S*-**7a**	86	97 (*R*)
2	*R*,*R*-**7b**	16[c]	91 (*S*)[d]
3	*S*,*S*-**7c**	97	99 (*R*)
4	*S*,*S*-**7d**	7	97 (*R*)
5	*R*,*R*-**7e**	97	97 (*S*)[d]
6	*R*,*R*-**7f**	80	99 (*S*)[d]
7	*R*,*R*-**7g**	16	98 (*S*)[d]

[a] Isolated yield after column chromatography. [b] Determined by HPLC analysis using Chiralpak ADH. [c] Reaction run for 48 h. [d] Opposite *S*-enantiomer produced.

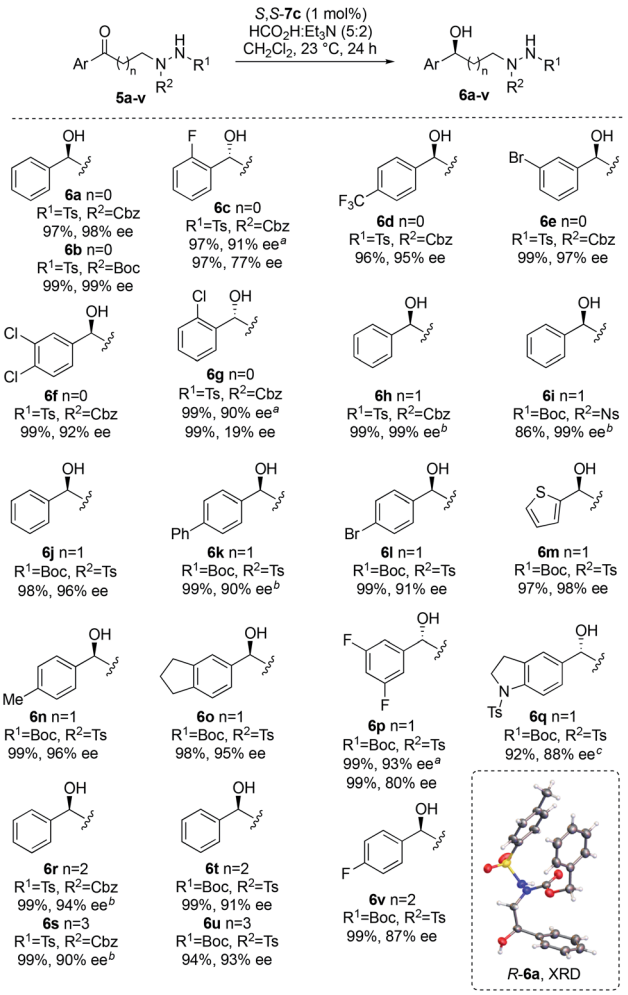

Fig. 2 Ru-catalyzed ATH of hydrazine-containing ketones. [a] Using *R,R*-**7f**. [b] ee determined after cyclization to **8**. [c] Using *R,R*-**7c**.

6a. For 2-substituted aryl derivatives **5c** and **5g**, and for 3,5-difluoro derivative **5p**, poor levels of stereoinduction were obtained using **7c** as catalyst. In these cases, use of **7f** bearing an additional electron-rich methoxy group on the arene significantly improved the enantioselectivity.[13b]

Ring closure of **6a–v** using diethyl azodicarboxylate (DEAD) and triphenylphosphine under Mitsunobu conditions provided the corresponding cyclic hydrazines **8a–v** in good to excellent yields (Fig. 3). It is possible to replace DEAD with less hazardous diisopropyl azodicarboxylate (DIAD), as illustrated by the cyclization of **6n** to **8n** and **6q** to **8q** with comparable efficiency. Furthermore, the methodology can be used to make either enantiomer of the cyclic hydrazine by use of catalyst *R,R*-**7c** or *S,S*-**7c**, as demonstrated by the synthesis of *R*-**8n** and *S*-**8n** (Fig. 3). Four- to seven-membered rings can conveniently be made using this method. In general, little or no loss in enantiopurity was seen during cyclization although for highly electron-rich thiophene **8m**, partial racemization (73% ee) was detected. The chemistry can be performed preparatively as illustrated by the synthesis of pyrazolidine *R*-**8j** on >5 g scale (see ESI†). In this case, the catalyst loading was halved to 0.5 mol%

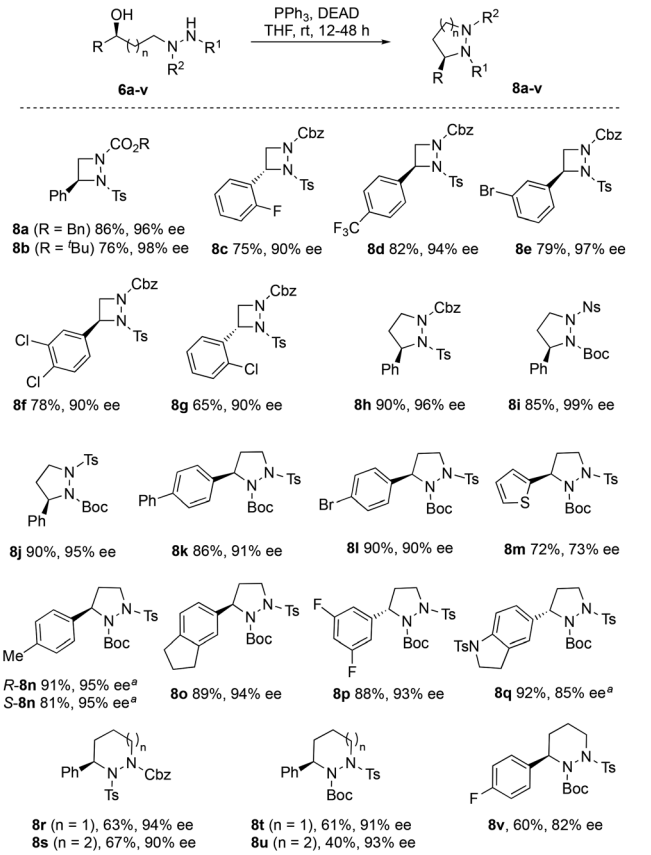

Fig. 3 Cyclic hydrazines **8a–v** made by Mitsunobu ring closure. [a] Reaction with DIAD in place of DEAD (for full details, see ESI†).

in the ATH step. No loss in ee was observed at this lower catalyst loading although longer reaction times (72 h) were required. For **8d** and **8h**, the structures were verified by XRD to confirm that stereochemical inversion occurred during cyclization (see ESI†).[14]

2.2. Synthesis of sp^3-rich hydrazine libraries by *N*-functionalization

To determine if these orthogonally-protected cyclic hydrazines could be used to generate sp^3-rich heterocyclic libraries, we explored their functionalization. To make this study practicable, a subset of six cyclic hydrazines, namely **8b**, **8j**, **8k**, and **8t–v**, were used. The sequence involved: (i) deprotection of the Ts group from the less hindered nitrogen using Mg metal; (ii) functionalization by C–N bond formation to introduce a variety of R^2 fragments; (iii) acidic deprotection of the Boc group from the second nitrogen; and (iv) addition of the R^1 fragment using similar chemistries used in step (ii) (Fig. 4). The deprotection reactions were essentially quantitative and so product purification was only conducted after each C–N functionalization. Conventional acylation and reductive amination reactions could be conducted on either nitrogen in generally high yields across a range of ring sizes. However, high-throughput optimization was required to identify general conditions for the Pd-catalyzed Buchwald–Hartwig arylations (for full details, see

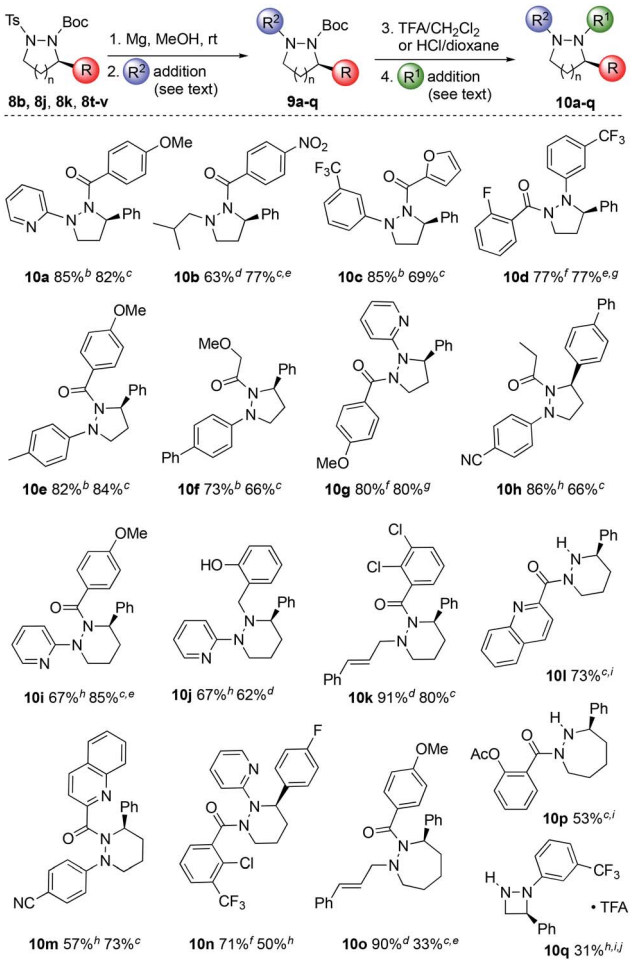

Fig. 4 *N*-Functionalization of enantioenriched cyclic hydrazines and hydrazides. [a] Isolated yields for two-step syntheses of **9** and **10** respectively. [b] ArBr, XPhosPd(crotyl)Cl (5 mol%), NaO*t*Bu, toluene, 90 °C, 20 h. [c] RCOCl, DIPEA, CH_2Cl_2, 0 °C to rt, 18 h. [d] RCHO, $NaBH(OAc)_3$, THF, rt, 20 h. [e] Enantiomeric excess determined by chiral HPLC. [f] RCOCl, CH_2Cl_2, rt, 18 h. [g] ArBr, BippyPhosPd(allyl)OTf (5 mol%), Cs_2CO_3, toluene, 90 °C, 20 h. [h] ArBr, $Pd(OAc)_2$ (5–10 mol%), Xantphos (10–20 mol%), NaO*t*Bu, toluene, 90 °C, 20 h. [i] Yield over 3 steps after Boc removal. [j] The Boc and Ts groups are transposed in the starting material **8b**.

ESI†). For the introduction of the R^2 fragment at the least hindered nitrogen on **8j**, XPhosPd(crotyl)Cl, NaO*t*Bu and toluene proved the most effective combination of catalyst, solvent and base. Cross-coupling of the more hindered nitrogen in the pyrazolidine ring was achieved with a BippyPhosPd(allyl)OTf catalyst to provide **10d** and **10g** in good yields. For other substrates differing in ring size and aryl group, $Pd(OAc)_2$ and Xantphos proved to be an effective catalyst system. Using this strategy, 14 derivatives (**10a–k**, **10m–o**) were produced bearing a diverse set of N- and C-substituents across different hydrazine ring sizes. Additionally, by omitting the final cross-coupling, scaffolds bearing free amines can also be produced (**10l**, **10p** and **10q**).[15] Four representative examples (**10b**, **10d**, **10i**, and **10o**) confirmed that no erosion of ee occurred during these functionalization sequences.

2.3. Molecular shape and dynamics of sp^3-rich hydrazine scaffolds

The shapes of the cyclic hydrazines have been studied using a combination of computational and spectroscopic tools. To assess the three-dimensionality of **10a–q** in the 17-member hydrazine library, the LLAMA package[16] was used to compute and display their principal moments of inertia (PMI) (Fig. 5).[17] This tool randomly selects a number of 3D-conformers for each molecule, minimizes their energy and selects the lowest-energy one. The selected minimum energy conformers of **10a–q** are provided in the ESI.† LLAMA then calculates the moments of inertia in the *x*, *y* and *z* axes. The PMI I1 coordinates are calculated by dividing inertia(*x*) by inertia(*z*). The I2 coordinates are calculated by dividing inertia(*y*) by inertia(*z*). This plot confirms that members of this small hydrazine library possess excellent shape diversity and three-dimensionality compared with conventional databases.[2] The wide distribution of the heterocycle frameworks within this plot suggests that it is the nature of the appended substituents (R, R^1 and R^2), rather than the size of the hydrazine ring, that has the greatest influence on their overall shape (Fig. 5).

Next, the solution and solid-state structures of representative cyclic hydrazines and hydrazides were determined. A total of eight derivatives were studied by single crystal X-ray diffraction (XRD).[14] The ORTEP depictions of **8d**, **9m**, **10a** and **10b** are given in Fig. 6. For four-membered **8d** and five-membered **10a** and **10b**, the *anti*,*anti*-configuration of the R, R^1 and R^2 substituents is apparent. For hexahydropyridazine **9m** where the conformational flexibility of the ring becomes more important, the R group still exerts a strong influence leading to a highly non-planar structure in which the R, R^1 and R^2 substituents are displayed in a predictable way on opposite faces of the hydrazine ring. The crystallographic data also provide insight into the extent of pyramidalization of the two nitrogen atoms within the ring,[18] a factor influencing both their shapes and fluxional behavior. The values for the pyramidalization of each nitrogen are given in Fig. 6, with larger values indicating more sp^3-character at the nitrogen center.

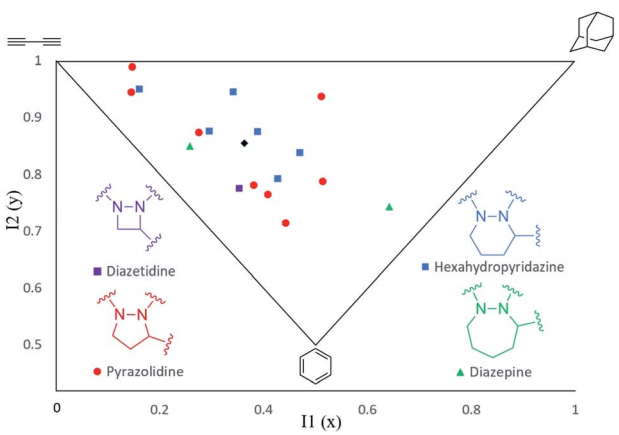

Fig. 5 Principal moments of inertia (PMI) plot of hydrazines **10a–q** indicating their molecular shapes. Mean PMI indicated (◆).

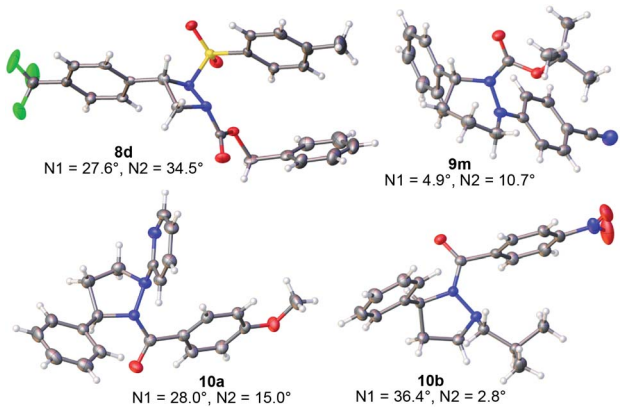

Fig. 6 Representative XRD structures of the cyclic hydrazines with measured values for the pyramidalization of the two ring nitrogens (N1 and N2).[18]

Next, the solution-state structure of **10b** was determined in C_6D_6 at 343 K by ^{1}H NOESY spectroscopy (600 MHz). These conditions were used to produce a *single* set of well resolved signals. The solution structure was assigned on the basis of NOESY cross-peaks between the *ortho*-hydrogens of the phenyl ring (H-3) and the methylene hydrogens of the isobutyl group (H-9 and possibly H-10) consistent with these substituents being on the same side of the hydrazine ring (Fig. 7b). Furthermore, the observation of a NOESY cross-peak between H-2 and H-8, and between H-6 and H-8 places all these atoms on the same side of the molecule and on the opposite face to the phenyl group (Fig. 7c). On this basis we assign an *anti*,*anti*-configuration to **10b** in solution (Fig. 7a), similar to the solid-state structure (Fig. 6).[14]

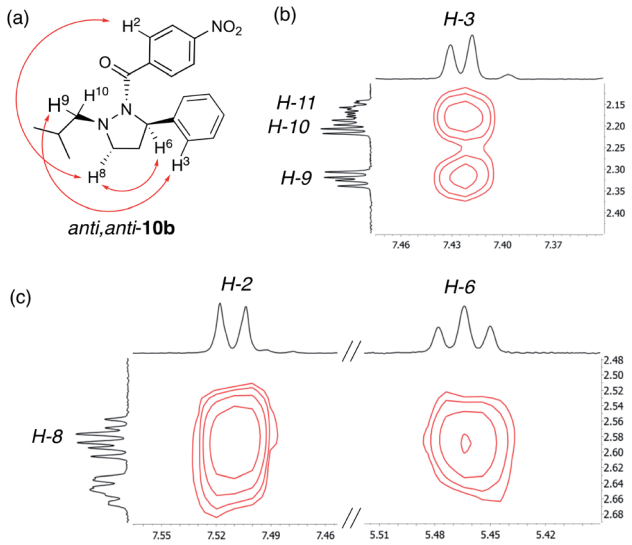

Fig. 7 Solution-state structure of **10b** derived by ^{1}H–^{1}H NOESY spectroscopy (600 MHz, C_6D_6, 343 K): (a) *anti*,*anti*-representation of **10b** with key NOEs indicated (red arrows). (b) Expansion of the NOESY spectrum highlighting cross-peaks between H-3 and H-9 and possibly H-10. (c) Expansion of the NOESY spectrum highlighting key cross-peaks between H-8 and H-2, and H-8 and H-6.

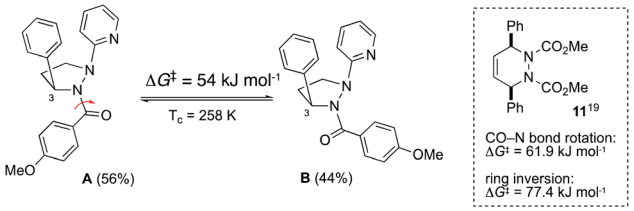

Scheme 2 Likely origin of fluxional behavior seen in **10a**.

To explore the fluxional behavior of the cyclic hydrazines, variable temperature ^{1}H NMR studies were conducted using **10a** and **10b**. For **10a**, the ^{1}H NMR spectrum resolved into two sharp sets of signals at 233 K in $CDCl_3$, indicating the presence of two conformational isomers in a 56 : 44 ratio. In contrast, **10b** exists predominately as a single conformational isomer at 233 K in $CDCl_3$ although small amounts of two additional isomers are seen (84 : 11 : 5). Evidently, the fluxional behavior is highly dependent on the nature of the N-substituents. This is consistent with changes in the extent of *N*-pyramidalization seen in the solid-state (Fig. 6). Using the resolved methyl singlets of **10a**, we were able to determine the barrier to interconversion of the two isomers at coalescence ($T_c = 258$ K, $\Delta G^{\ddagger} = 54$ kJ mol^{-1}, see ESI†). The question arises as to whether the two isomers come from fluxionality at the hydrazine centers (Scheme 1), or from a process such as amide bond rotation within *anti*,*anti*-**10a**? On the available evidence, we suggest that only amide rotamers are being observed *i.e.* **A** and **B** (Scheme 2). Firstly, whilst low temperature NOESY experiments did not allow us to fully deduce the solution-state structure of **10a**, we did observe a NOESY cross-peak between the methine hydrogen at H-3 and the *ortho*-hydrogens of the CO*Ar* group for **A** but not **B** consistent with this assignment. Secondly, the measured interconversion barrier is more consistent with that of an amide bond rotation in similar systems. For example, both types of fluxionality operate concurrently in **11** with a lower barrier for rotation about the N–CO bond than ring inversion (box insert, Scheme 2).[19] Finally, the near equal population of **A** and **B** is inconsistent with N-inversion as **1b–d** are expected to be higher energy species due to unfavorable non-bonded interactions (Scheme 1). Although *N*-fluxionality is not operating in **10a**, the observation of a third set of signals for **10b** at low temperature, suggests that conformational isomers arising from N-inversion are accessible for some systems, albeit in low concentrations.

3. Conclusions

An efficient synthesis of differentially-protected cyclic hydrazines containing an adjacent stereogenic carbon atom has been devised using ATH as the key step. Commercially available tethered Ru-catalyst **7c**, available in both enantiomeric forms, proved highly effective for the introduction of the asymmetric center by ketone reduction. In the few cases where low enantioselectivity was seen in the ATH, tethered catalyst **7f** gave further improvements. The methodology was used to make 22 different cyclic hydrazines in up to 99% ee, through variation in

ring size (4- to 7-membered rings), C-3 substituents and nitrogen protecting groups. The chemistry is operationally simple and can be performed on a preparative scale. Chemical library construction is possible from these hydrazines by iterative C–N bond formation. Wide chemical diversification is possible through variation in the hydrazine structure, use of different functionalization chemistries and coupling partners, and controlled engagement of each nitrogen of the hydrazine in turn. Principal moment of inertia (PMI) analysis revealed excellent shape diversity and three-dimensionality within the assembled library, indicating their potential value in drug discovery. The preference for the molecules to adopt *anti*,*anti*-orientations of the three stereocenters was established using a combination of XRD and NMR spectroscopy. The fluxional behavior of these compounds was further explored by VT-NMR and low temperature NOESY experiments, from which useful insights have emerged about how the molecules sample chemical space. Future work will examine the feasibility of making larger chemical libraries based on these non-planar scaffolds and the exploitation of this chemistry in drug discovery programs.

Conflicts of interest

There are no conflicts to declare.

Acknowledgements

We thank the Leverhulme Trust (RPG-2014-362), Eli Lilly and the University of Warwick for generous financial support, and Johnson Matthey for the gift of tethered catalysts **7c–e**. Crystallographic data were collected using an instrument that received funding from the European Research Council under the European Union's Horizon 2020 research and innovation program (grant agreement No. 637313). We gratefully acknowledge the help of Dr Ivan Prokes (University of Warwick) with the NMR experiments.

Notes and references

1 For reviews, see: (*a*) A. Karawajczyk, F. Giordanetto, J. Benningshof, D. Hamza, T. Kalliokoski, K. Pouwer, R. Morgentin, A. Nelson, G. Müller, A. Piechot and D. Tzalis, *Drug Discovery Today*, 2015, **20**, 1310–1316; (*b*) F. Lovering, J. Bikker and C. Humblet, *J. Med. Chem.*, 2009, **52**, 6752–6756; (*c*) T. J. Ritchie and S. J. F. Macdonald, *Drug Discovery Today*, 2009, **14**, 1011–1020.

2 J. Meyers, M. Carter, N. Y. Mok and N. Brown, *Future Med. Chem.*, 2016, **8**, 1753–1767.

3 For selected examples, see: (*a*) B. L. Donnelly, L. D. Elliott, C. L. Willis and K. I. Booker-Milburn, *Angew. Chem., Int. Ed.*, 2019, **58**, 9095–9098; (*b*) A. Sveiczer, A. J. P. North, N. Mateu, S. L. Kidd, H. F. Sore and D. R. Spring, *Org. Lett.*, 2019, **21**, 4600–4604; (*c*) N. J. Flodén, A. Trowbridge, D. Willcox, S. M. Walton, Y. Kim and M. J. Gaunt, *J. Am. Chem. Soc.*, 2019, **141**, 8426–8430; (*d*) T.-G. Chen, L. M. Barton, Y. Lin, J. Tsien, D. Kossler, I. Bastida, S. Asai, C. Bi, J. S. Chen, M. Shan, H. Fang, F. G. Fang, H.-W. Choi, L. Hawkins, T. Qin and P. S. Baran, *Nature*, 2018, **560**, 350–354; (*e*) D. J. Foley, P. G. E. Craven, P. M. Collins, R. G. Doveston, A. Aimon, R. Talon, I. Churcher, F. von Delft, S. P. Marsden and A. Nelson, *Chem.–Eur. J.*, 2017, **23**, 15227–15232; (*f*) R. Gianatassio, J. M. Lopchuk, J. Wang, C.-M. Pan, L. R. Malins, L. Prieto, T. A. Brandt, M. R. Collins, G. M. Gallego, N. W. Sach, J. E. Spangler, H. Zhu, J. Zhu and P. S. Baran, *Science*, 2016, **351**, 241–246; (*g*) B. A. Chalmers, H. Xing, S. Houston, C. Clark, S. Ghassabian, A. Kuo, B. Cao, A. Reitsma, C.-E. P. Murray, J. E. Stok, G. M. Boyle, C. J. Pierce, S. W. Littler, D. A. Winkler, P. V. Bernhardt, C. Pasay, J. J. De Voss, J. McCarthy, P. G. Parsons, G. H. Walter, M. T. Smith, H. M. Cooper, S. K. Nilsson, J. Tsanaktsidis, G. P. Savage and C. M. Williams, *Angew. Chem., Int. Ed.*, 2016, **55**, 3580–3585; (*h*) M. U. Luescher and J. W. Bode, *Org. Lett.*, 2016, **18**, 2652–2655.

4 For a reviews, see: (*a*) G. Le Goff and J. Ouazzani, *Bioorg. Med. Chem.*, 2014, **22**, 6529–6544; (*b*) E. Licandro and D. Perdicchia, *Eur. J. Org. Chem.*, 2004, 665–675.

5 K. C.-C. Cheng, S. Cao, A. Raveh, R. MacArthur, P. Dranchak, G. Chlipala, M. T. Okoneski, R. Guha, R. T. Eastman, J. Yuan, P. J. Schultz, X.-Z. Su, G. Tamayo-Castillo, T. Matainaho, J. Clardy, D. H. Sherman and J. Inglese, *J. Nat. Prod.*, 2015, **78**, 2411–2422.

6 V. A. Steadman, S. B. Pettit, K. G. Poullennec, L. Lazarides, A. J. Keats, D. K. Dean, S. J. Stanway, C. A. Austin, J. A. Sanvoisin, G. M. Watt, H. G. Fliri, A. C. Liclican, D. Jin, M. H. Wong, S. A. Leavitt, Y.-J. Lee, Y. Tian, C. R. Frey, T. C. Appleby, U. Schmitz, P. Jansa, R. L. Mackman and B. E. Schultz, *J. Med. Chem.*, 2017, **60**, 1000–1017 and references cited therein.

7 M. P. Clark, S. K. Laughlin, M. J. Laufersweiler, R. G. Bookland, T. A. Brugel, A. Golebiowski, M. P. Sabat, J. A. Townes, J. C. VanRens, J. F. Djung, M. G. Natchus, B. De, L. C. Hsieh, S. C. Xu, R. L. Walter, M. J. Mekel, S. A. Heitmeyer, K. K. Brown, K. Juergens, Y. O. Taiwo and M. J. Janusz, *J. Med. Chem.*, 2004, **47**, 2724–2727.

8 F. Deget and R. N. Brogden, *Drugs*, 1991, **41**, 799–820.

9 For examples, see: (*a*) M. Kamuf and O. Trapp, *Chirality*, 2013, **25**, 224–229; (*b*) A. Perjéssy, P. Meyer, W.-D. Rudorf, D. Loos, E. Kolehmainen, K. Laihia, M. Nissinen, J. Koivisto and R. Kauppinen, *J. Phys. Org. Chem.*, 2001, **14**, 811–818; (*c*) R. G. Kostyanovsky, G. K. Kadorkina, V. R. Kostyanovsky, V. Schurig and O. Trapp, *Angew. Chem., Int. Ed.*, 2000, **39**, 2938–2940; (*d*) J. E. Anderson, *J. Am. Chem. Soc.*, 1969, **91**, 6374–6380.

10 For selected examples, see: (*a*) X. Kou, Q. Shao, C. Ye, G. Yang and W. Zhang, *J. Am. Chem. Soc.*, 2018, **140**, 7587–7597; (*b*) S. Rajkumar, G. J. Clarkson and M. Shipman, *Org. Lett.*, 2017, **19**, 2058–2061; (*c*) A.-S. Marques, M. Giardinetti, J. Marrot, V. Coeffard, X. Moreau and C. Greck, *Org. Biomol. Chem.*, 2016, **14**, 2828–2832; (*d*) H.-J. Leng, F. Peng, S. Zingales, W. Huang, B. Wang, Q. Zhao, R. Zhou, G. He, C. Peng and B. Han, *Chem.–Eur. J.*, 2015, **21**, 18100–18108; (*e*) D.-Y. Zhang, L. Shao, J. Xu

and X.-P. Hu, *ACS Catal.*, 2015, **5**, 5026–5030; (*f*) L. Lykke, B. D. Carlsen, R. S. Rambo and K. A. Jørgensen, *J. Am. Chem. Soc.*, 2014, **136**, 11296–11299; (*g*) M. Fernández, E. Reyes, J. L. Vicario, D. Badía and L. Carrillo, *Adv. Synth. Catal.*, 2012, **354**, 371–376; (*h*) R. L. LaLonde, Z. J. Wang, M. Mba, A. D. Lackner and F. D. Toste, *Angew. Chem., Int. Ed.*, 2010, **49**, 598–601.

11 For reviews, see: (*a*) H. G. Nedden, A. Zanotti-Gerosa and M. Wills, *Chem. Rec.*, 2016, **16**, 2623–2643; (*b*) D. Wang and D. Astruc, *Chem. Rev.*, 2015, **115**, 6621–6686; (*c*) F. Foubelo, C. Nájera and M. Yus, *Tetrahedron: Asymmetry*, 2015, **26**, 769–790; (*d*) R. Noyori and S. Hashiguchi, *Acc. Chem. Res.*, 1997, **30**, 97–102.

12 L. Grehn, B. Nyasse and U. Ragnarsson, *Synthesis*, 1997, 1429–1432.

13 (*a*) A. M. Hayes, D. J. Morris, G. J. Clarkson and M. Wills, *J. Am. Chem. Soc.*, 2005, **127**, 7318–7319; (*b*) R. Soni, K. E. Jolley, G. J. Clarkson and M. Wills, *Org. Lett.*, 2013, **15**, 5110–5113; (*c*) R. Hodgkinson, V. Jurčík, A. Zanotti-Gerosa, H. G. Nedden, A. Blackaby, G. J. Clarkson and M. Wills, *Organometallics*, 2014, **33**, 5517–5524; (*d*) R. Soni, K. E. Jolley, S. Gosiewska, G. J. Clarkson, Z. Fang, T. H. Hall, B. N. Treloar, R. C. Knighton and M. Wills, *Organometallics*, 2018, **37**, 48–64.

14 CCDC 1944266 (**6a**), 1944267 (**8d**), 1944268 (**8h**), 1944269 (**10a**), 1944270 (**10b**), 1944271 (**9m**), 1944272 (**10l**), 1944273 (**9i**), and 1955341 (**10o**) contain the supplementary crystallographic data for this paper.†

15 Double functionalization of four-membered diazetidines such as **8b** has proven difficult in part because of low yields in the Pd-catalyzed cross-couplings. After N-deprotection, such substrates have more limited chemical stability.

16 I. Colomer, C. J. Empson, P. Craven, Z. Owen, R. G. Doveston, I. Churcher, S. P. Marsden and A. Nelson, *Chem. Commun.*, 2016, **52**, 7209–7212.

17 E. Lenci and A. Trabocchi, *ChemBioChem*, 2019, **20**, 1115–1123.

18 The pyramidalization of the nitrogen atoms is defined as $360 - \Sigma$ where Σ is the sum of the valence angles of the nitrogen atom.

19 J. E. Anderson and J. M. Lehn, *Tetrahedron*, 1968, **24**, 137–149.